MD Simulations and Experimental Study of Structure, Dynamics, and Thermodynamics of Poly(ethylene oxide) and Its Oligomers

Oleg Borodin,*,† Richard Douglas,† Grant D. Smith,†,‡ Frans Trouw,§ and Sergio Petrucci#

Department of Materials Science and Engineering, 122 S. Central Campus Drive, Rm. 304, University of Utah, Salt Lake City, Utah 84112, Manuel Lujan Jr. Neutron Scattering Center, MS H805, Los Alamos National Laboratory, New Mexico 87545, Department of Chemical and Fuels Engineering, University of Utah, Salt Lake City, Utah 84112, and Polytechnic University, Farmingdale, New York 11735

Molecular dynamics (MD) simulations have been performed on poly(ethylene oxide) (PEO) and its oligomers, using quantum chemistry-based force fields with and without many-body polarizable interactions. Inclusion of the many-body polarization in the model resulted in increased populations of the tgt and tgg conformations of 1,2-dimethoxyethane and slightly slower dynamics. Increasing the PEO dipole moment also led to increased populations of the tgt and ttg conformers and slower dynamics. Quasi-elastic neutron scattering, dielectric relaxation, and ^{13}C spin−lattice relaxation experiments have been performed on PEO and its oligomers. New ^{13}C NMR experiments yielded spin−lattice relaxation times that were ∼2−3 times larger than those in the previous experiments, which is in good agreement with the current simulation results. Good agreement between the MD simulation results using many-body polarizable and two-body nonpolarizable potentials was found with experiments for thermodynamic, transport, structural, and dynamic properties.

I. Introduction

Poly(ethylene oxide) (PEO) is an ubiquitous polymer that is used in a wide range of technologically important applications, such as polymer electrolytes, protein partitioning, drug delivery, and aqueous biphasic separation, which has been briefly described in ref 1. We are particularly interested in gaining insight into ion transport and developing predictive tools for understanding the structure−property relationship in polymer electrolytes that are comprised of a PEO-based matrix that has been doped with lithium salts. Accurate description of the structural and dynamic properties of PEO melts and PEO/Li$^+$ interactions is important for the accurate modeling of polymer electrolytes. To systematically approach the development of the polymer electrolyte atomistic model, e.g., the PEO/Li salt force field, we initiated a study that has been summarized in a three-paper series[1,2] that involves systematic developments of quantum chemistry-based force fields for polymer melts and polymer−salt solutions, force field validation, and studies of the structure−property relationship in polymer electrolytes. This paper is the second in the series.

In the first paper,[1] we developed the two-body (TB) nonpolarizable and many-body (MB) polarizable quantum chemistry-based force fields for PEO, with the purpose of using this force field for polymer electrolyte modeling.[2] The many-body polarizable interactions have been included in the PEO force field, because they are expected to have a significant contribution to the PEO/Li$^+$ complexation energetics and some effect on the structure and dynamics of PEO melts. Investigation of the effect of the many-body polarization on conformational and dynamic properties of PEO melts is presented in this paper, whereas the effect of the many-body polarizable interactions on ion transport and the structure of the polymer electrolytes will be discussed in the next paper.[2] In this contribution, we also discuss the influence of the choice of partial charges representing the electrostatic potential around PEO on the conformational and dynamic properties of PEO melts and its oligomers. The reason for this investigation is the inability of the partial charge model to represent, with high accuracy (<1%−5%), the electrostatic potential close to and far from ether molecules, using one set of partial charges. For example, a simple least-squares fit to the electrostatic potential around PEO oligomers (e.g., ethers) provided a good fit to the electrostatic potential far from atoms (at a distance of >3 Å) but underestimated the electrostatic potential at a point of the expected Li$^+$ complexation to the 1,2-dimethoxyethane (DME) tgt conformer by ∼10 kcal/mol, out of 50 kcal/mol, as shown in Figure 3 of ref 1. The PEO force field with such a description of the electrostatic potential cannot be used for the accurate prediction of DME/Li$^+$ or PEO/Li$^+$ complexation energetics. Increased weighting of the electrostatic potential at grid points close to the ether atoms during fitting improved the description of the electrostatic potential in the proximity of a molecule, allowing for more-accurate description of the DME/Li$^+$ and PEO/Li$^+$ complexation energies, but at the expense of overestimating the electrostatic potential far from the DME molecule. Thus, various compromises between accurate descriptions in the proximity of a molecule and far from it are possible. In this contribution, we have used two sets of partial charges. The first set of partial charges was obtained by fitting the electrostatic potential from the force field to that from quantum chemistry, using the absolute value of the electrostatic potential to weight the contribution of grid points during fitting (ϕ-weighting), whereas the second set of partial charges was obtained in a similar manner but with the square of the electrostatic potential used

* Author to whom correspondence should be addressed. E-mail: e-mail: Oleg.Borodin@utah.edu.
† Department of Materials Science and Engineering, University of Utah.
‡ Department of Chemical and Fuels Engineering.
§ Los Alamos National Laboratory.
# Polytechnic University.

TABLE 1: Summary of Differences between Quantum Chemistry-Based Potentials Used in This Work

force field	weighting function used to weight grid points in the least-squares fitting of partial charges to reproduce electrostatic grid around PEO oligomers	torsional potential were fit to:
FF-1	absolute value of the electrostatic potential (ϕ)	quantum chemistry energetics
FF-2	a square of the electrostatic potential (ϕ^2)	quantum chemistry energetics
FF-3	a square of the electrostatic potential (ϕ^2)	quantum chemistry energetics with barriers lowered by 0.3−0.9 kcal/mol

for weighting grid point contribution to the electrostatic potential during fitting (ϕ^2-weighting) (see Table 1 and ref 1). The first set of charges used in the FF-1 force fields represents a compromise between descriptions of the electrostatic grip close to and far from PEO oligomers. The quantum chemistry-based FF-1 force field, using this set of partial charges, together with the other quantum chemistry-based parameters, will be shown to give a PEO melt structure and dynamics that are in good agreement with experiments. However, underestimation of the PEO/Li$^+$ complexation energy by the FF-1 force field puts its use for polymer electrolyte modeling in question. The second set of partial charges aims for an accurate description of the PEO/Li$^+$ complexation energy while overestimating the ether dipole moments (by 16%) and electrostatic potential far from the molecule. The FF-2 force field, using this second set of partial charges, will be shown to yield PEO dynamics that are ∼10%−30% slower than the first set of charges, requiring empirical adjustments to the torsional potential to accelerate the polymer dynamics and improve the agreement with experiments and molecular dynamics (MD) results using the FF-1 force field. The force field with these empirical adjustments will be called the FF-3 force field. Table 1 briefly summarizes the differences between the force fields.

In this contribution, we report MD simulations of PEO and its oligomers, using these force fields (FF-1, FF-2, and FF-3 MB polarizable force fields and TB nonpolarizable force fields) to (a) investigate the effect of many-body polarizable interaction on the PEO conformations, structure, and dynamics; (b) explore the influence of the choice of partial charges on the PEO conformations, structure, and dynamics; and (c) validate the quantum chemistry-based force fields against experimental data. New quasi-elastic neutron scattering (QNS), dielectric spectroscopy, and ^{13}C spin−lattice relaxation NMR experiments have been performed on PEO and its oligomers to validate the force fields and resolve inconsistencies in some previously published experimental data with MD simulations results and the other experiments.

II. Previous MD Simulations of PEO

Several PEO force fields have been employed in MD simulations of PEO, its oligomers, and PEO-based polymer electrolytes.[3−8] None of these models have included many-body polarizable interactions. Previous MD simulations by Smith et al.[5] with a quantum chemistry-based force field yielded the correct temperature dependence of the PEO characteristic ratio and the characteristic ratio itself ($C_\infty = 5.5 \pm 0.3$),[9,10] as well as structure factors,[11] the position of the maximum of the dielectric loss spectra,[12] and spin−lattice relaxation times[12] (T_1) that are in good agreement with the experiment. However, the ^{13}C spin−lattice relaxation times from NMR experiments reported in this manuscript differ considerably from the previously reported values,[12] indicating that the PEO dynamics predicted by that force field are somewhat slow. This issue will be addressed in this work.

The Neyertz et al.[6,13] force field was validated against the available crystal PEO data. They found a PEO characteristic ratio of 5.5, which was in good agreement with experiments,[10] but their abundant populations of g$^+$g$^-$g$^+$ is inconsistent with our quantum chemistry results, which casts doubt on the accuracy of their force field, as discussed in ref 9. Halley et al.[3] compared the structure factor for the PEO from MD simulations with that from the experiment, achieving only limited success. The de Leeuw group used a modified version of the Neyertz et al.[6] force field in their MD simulations of PEO oligomers and found good agreement for the intermediate incoherent structure factor between MD simulations and neutron spin−echo (NSE) experiments.[14] Other groups[4,6,8] limited their validation of their PEO simulations to comparing the densities from MD simulations and experiments, making it difficult to judge the ability of the force fields used to reproduce polymer structural and dynamical properties.

III. Experimental Section

A. Quasi-elastic Neutron Scattering Measurements on PEO. Poly(ethylene glycol) dimethyl ether, or "PEO-500", was used for the neutron scattering experiments at a temperature of 318 K. The polymer used was relatively polydisperse ($M_w = 470$, $M_n = 398$), as obtained from Aldrich, and was used as received. The QNS experiments were performed on the disk chopper spectrometer (DCS) that is located at the NIST Center for Neutron Research (http://www.ncnr.nist.gov). This direct geometry chopper spectrometer was operated with an incident neutron wavelength of 0.48 nm, which yielded an energy resolution function that is approximately Gaussian in shape, with a full width at half-maximum of 105 μeV. An annular sample geometry was chosen for this experiment, in an attempt to reduce the multiple scattering in a thick sample. An aluminum sample can that was composed of two concentric cans was used, with an approximate diameter of 1.98 cm and an annular gap of 0.04 cm. The sample can was mounted to a closed-circuit refrigerator that was equipped with a heater to allow for sample control at 318 K. A more detailed description of the measurements and data analysis is reported elsewhere.[15] Sample loading was performed under an argon atmosphere.

B. Quasi-elastic Neutron Scattering Measurements on 1,2-Dimethoxyethane. These experiments were conducted at the Intense Pulse Neutron Source Division of the Argonne National Laboratory, using the QNS spectrometer,[16] which is a "crystal-analyzer" or "inverse-geometry" spectrometer that accepts a white beam from a solid methane moderator onto the sample. Constant-energy focusing of the graphite analyzer crystal arrays provides for an energy resolution of ∼100 μeV for the quasi-elastic and low-energy inelastic scattering. The complete scan using the rotating table yields nine spectra, covering the momentum transfer range from 0.5 to 2.5 Å^{-1}. 1,2-Dimethoxy-ethane (DME) was purchased from Aldrich and used without further purification. The samples were evenly distributed in a cylindrical aluminum envelope, to minimize sample thickness and, thus, reduce multiple scattering, and were placed in a circular thin aluminum cylinder ∼12 cm long and 0.7 cm in diameter. An indium gasket seal was used to keep the sample in the container, because the sample is placed in a vacuum
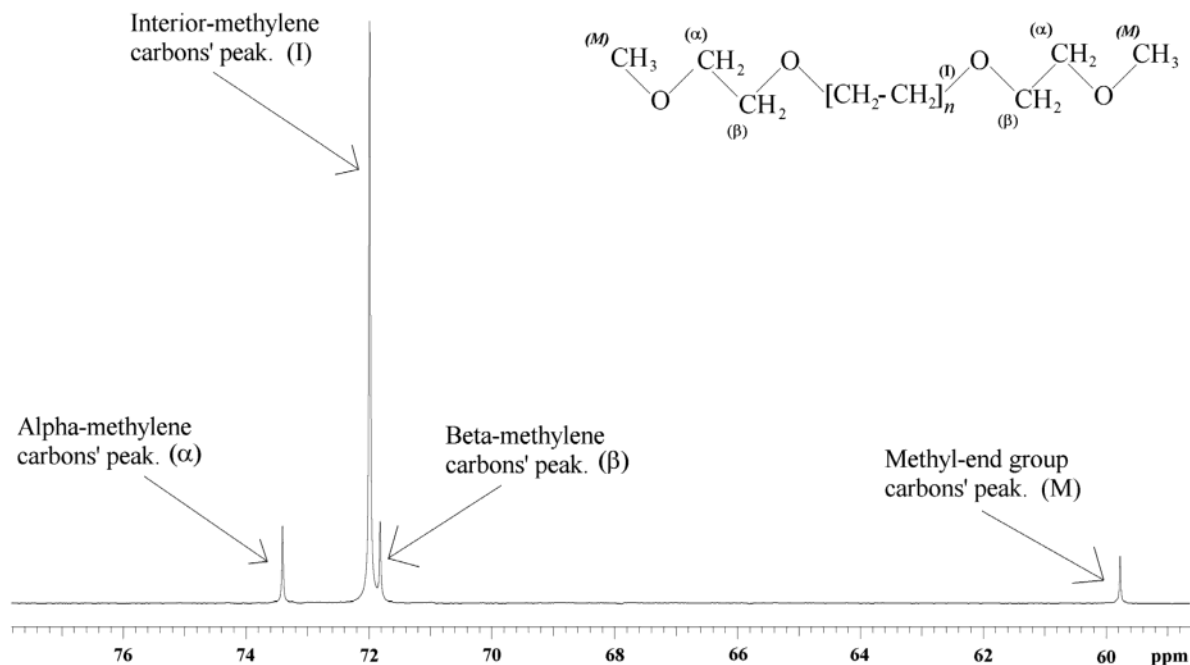
Structure, Dynamics, and Thermodynamics of PEO

J. Phys. Chem. B, Vol. 107, No. 28, 2003 **6815**

Figure 1. Structure of ^{13}C NMR spectrum of neat PEO.

during the experiment. Experiments were performed at 318 K. Typical data collection time was 6–8 h. The time-of-flight data were then transformed via the neutron scattering law, $S(Q,\omega)$, using the standard conversion programs, as described in ref 17. A fast Fourier transform was used to convert $S(Q,\omega)$ to an intermediate scattering function, $I(Q,t)$.[17]

C. ^{13}C Spin-Lattice NMR Measurements. Measurement of the ^{13}C-proton-decoupled NMR at a resonance frequency of 500 MHz was conducted on PEO-500 ($M_w = 470$, $M_n = 398$; Lot No. 02114CO) and another poly(ethylene glycol) dimethyl ether ("PEO-2000", $M_w = 1854$, $M_n = 1733$; Lot No. 350765/1), each of which were obtained from Aldrich and used without further purification. PEO readily absorbs water vapor, oxygen gas, and carbon dioxide gas from the atmosphere, causing unwanted changes that would have an unfavorable presence in experimental results; therefore, all PEO samples were subjected to several freeze–thaw cycles, under vacuum inside the transfer chamber of a dry glovebox operated in an atmosphere of nitrogen gas. After the sample tubes were prepared, they were capped with plastic lids and then flame-sealed with a propane–oxygen torch, to avoid any future contamination.

The ^{13}C NMR experiments utilized an Inova 500 MHz spectrometer with a 5-mm pulsed-field-gradient (PFG) switchable broadband probe. Pyrex glass NMR sample tubes (5.0 mm–528pp, 7 in. long) from the Wilmad/Lab Glass Company were used. T_1 values were measured by the inversion recovery method, with the 180°-perturbation pulse width calibrated to produce a zero-intensity resonant peak spectrum. Each spectrum obtained was the average of four transients, and a line broadening of 2 Hz was used in the processing of the free induction decay. At the time of the experiment, the variable-temperature controller of the NMR equipment was not calibrated. However, later tests using a ethylene glycol standard demonstrated that the temperature controller was accurate to ±3 °C.

At 500 MHz, the ^{13}C-proton decoupled spectrum revealed four distinguishable resonance peaks, as shown in Figure 1. The most prominent peak was due to the resonance signals of multiple interior carbon atoms only, excluding the three carbon atoms on both ends. The remaining three, less-intense resonance

peaks are each caused by the carbon atoms at PEO chain ends and the end methyl carbon groups (namely, the methyl-, α-, and β-carbon atoms, working inward from the ends, respectively). The chemical-shift anisotropy observed along the ends of the PEO chains is greatest for the methyl end groups, which also exhibit the longest relaxation times. This trend continues inward to the α- and β-carbon atoms, as well as all other interior carbon atoms, becoming less significant the farther inward the carbon atom is, relative to the end methyl carbon group.

The relaxation time T_1 for any resonance peak in the spectrum is characterized as the time required for the peak to return to thermal equilibrium after the fully intense peak is completely inverted by a 180° perturbation pulse. Varian software that was applied in conjunction with the NMR device was used to determine the T_1 relaxation times via the inversion recovery method. This method employs a graphical representation of an array of different spectra, each having different relative peak intestines, or peak heights, as a function of delay time. The delay time is the time allocated for relaxation before acquisition of the spectrum. The software then performs a nonlinear regression to converge, within a 95% confidence interval, on a value for T_1 as an inverse decay constant into a standard exponential spin–lattice decay function, which best fits the curve to match the peak intensity decay pattern for the spectral array. The errors in the reported T_1 values are the standard deviation from actual peak intensities to those obtained by the nonlinear regression from the empirically fit decay function (also done using the Varian NMR software).

D. Dielectric Spectroscopy Experiments. PEO-500 ($M_w = 470$, $M_n = 398$) was obtained from Fluka and dried over a molecular sieve. The equipment and procedure for the dielectric measurements have been described previously.[18,19] All the sample manipulations were performed in a glovebox that was filled with dry nitrogen.

E. Viscosity Measurements. Viscosity measurements were performed at 318–363 K on PEO-500 ($M_w = 470$, $M_n = 398$) that had been obtained from Aldrich and used without further purification. Two independent sets of measurements were performed, using a Brookfield rotating viscometer and a Cannon-Fenske type, slanted-tube capillary viscometer that was

calibrated with distilled water and standard oil S6 (No. 84104). Results of the measurements were in agreement, to within 2%.

IV. MD Simulations Methodology

MD simulations were performed on CH_3-capped oligomers of ethylene oxide (H−$(CH_2$−O−$CH_2)_n$−H, for n = 1, 2, 3, ..., 54) and a polydisperse system with M_n = 398 and M_w = 475 (referenced in this paper as PEO-500). The linear dimension of the simulation cubic box varied from 23.5 Å to 34 Å, depending on the system. The MD simulations code Lucretius was used.[20] All systems were created in the gas phase. The box was shrunk in MD simulations, using a Brownian dynamics algorithm[21] over a period of 1−3 ns to yield the experimental densities, with subsequent equilibration in the NPT ensemble for 0.5−5 ns, using the velocity Verlet algorithm with a time step of 1 fs.[22] A 1-ns constant pressure run was performed at each temperature, to determine the equilibrium density. Subsequent sampling runs in an NVT ensemble were 1−45 ns in duration. Table 1 summarizes the run lengths for ethylene oxide with n = 1, 2, and 3 and PEO-500, whereas the NVT runs for n = 54 were 25 ns at 393 K (the FF-3 force field) and 15 ns for the FF-1 and FF-2 force fields, and 15 ns at 343 K for all force fields. A Nose−Hoover thermostat[23] and a barostat[24] were used to control the temperature and pressure, whereas bond lengths were constrained using the Shake algorithm.[25] The Ewald summation method[26] was used for treatment of long-range electrostatic forces between partial charges with partial charges and partial charges with induced dipoles for the many-body polarizable potential, and the particle-mesh Ewald (PME) technique[27] was used for the simulations using the two-body nonpolarizable potential. A tapering function[28] was used to drive induced dipole−induced dipole interactions to zero at the cutoff of 10 Å. A multiple-time-step reversible reference system propagator algorithm was employed,[29] with a time step of 0.75 fs for bonding, bending, and torsional motions, a time step of 1.5 fs for nonbonded interactions within a 6.5 Å sphere, and a time step of 3.0 fs for nonbonded interactions within 6.5−10.0 Å and the reciprocal space part of the Ewald and PME summation.

V. Property Calculation from MD Simulations

A. Enthalpy of Vaporization. Heats of vaporization (ΔH) were calculated using eq 1:

$$\Delta H = U^{liq} - U^{vap} + RT \qquad (1)$$

where U^{liq} and U^{vap} are the energies of the liquid and gas phases, respectively, R is the gas constant, and T is temperature. The gas-phase energy was calculated in MD simulations using Brownian dynamics and no intermolecular interactions.

B. Static Structure Factor. The static structure factor was calculated using eq 2:

$$S(Q) = \\ 1 + \left(\frac{1}{\langle b \rangle^2}\right) n \sum_{\alpha,\beta} x_\alpha b_\alpha x_\beta b_\beta \int_0^{r_c} (g_{\alpha\beta}(r) - 1)\left(\frac{\sin Qr}{Qr}\right) 4\pi r^2 \, dr \quad (2)$$

where $\langle b \rangle^2 \equiv \sum_\alpha x_\alpha x_\beta b_\alpha b_\beta$, n is a number density, $g_{\alpha\beta}(r)$ is the radial distribution function (RDF) for α/β atom types, Q is the wave vector, b_α and b_β are the coherent scattering length for species α and β, x_α and x_β are the fraction of atom types α and β, and r_c is the cutoff for integration (15 Å).

C. Intermediate Incoherent Dynamic Structure Factor. For isotropic systems such as liquids, the neutron scattering incoherent intermediate scattering function (ISF), $I(Q,t)$, is given by eq 3:[30]

$$I_{inc}(Q,t) = \left\langle \frac{\sin(\Delta r_i(t)Q)}{\Delta r_i(t)Q} \right\rangle \qquad (3)$$

where $\Delta r_i(t)$ is the displacement of atom i after time t, Q is the magnitude of the momentum transfer vector, and the angled brackets denote an average over all time origins for atoms with a significant incoherent cross section (i.e., hydrogen atoms).

D. Frequency-Dependent Dielectric Constant. Linear response theory allows us to obtain the complex dielectric permittivity $\epsilon^*(\omega) = \epsilon' + i\epsilon''$ for the PEO melt, using the relationship[31]

$$\frac{\epsilon' + i\epsilon''}{\Delta\epsilon} = 1 - i\omega \int_0^\infty \Phi(t) \exp(-i\omega t) \, dt \qquad (4)$$

where the dipole moment autocorrelation function (DACF) is given by

$$\Phi(t) = \frac{\langle \mathbf{M}(0)\cdot\mathbf{M}(t) \rangle}{\langle \mathbf{M}(0)\cdot\mathbf{M}(0) \rangle} \qquad (5)$$

where $\Delta\epsilon$, the relaxation strength, is equal to $\epsilon_r - \epsilon_u$. Here, $\mathbf{M}(t)$ is the dipole moment of the system at time t, V the volume of the system, k_B the Boltzmann constant, and T the temperature. The angled brackets ($\langle \rangle$) denote an ensemble average. The unrelaxed dielectric constant (ϵ_u) is the dielectric constant that includes all relaxation processes at frequencies higher than the process of interest, i.e., electronic polarization and relaxation due to vibrations and librations, whereas the relaxed dielectric constant (ϵ_r) is the value obtained after the relaxation process (i.e., dipole orientational relaxation) is complete.

E. Spin-Lattice NMR Relaxation Times (T_1). NMR spin−lattice relaxation times (T_1) probe the rate of decay of the C−H vector, which is related to polymer dynamics. The T_1 spin−lattice relaxation times for the carbon nuclei associated with the methyl-, α-, and β-carbon atoms, as well as the interior carbon atoms, were measured and labeled according to Figure 1. The experimentally determined T_1 values are related to the microscopic motion of the C−H vectors through the relationship[32]

$$\frac{1}{nT_1} = K[J(\omega_H - \omega_C) + 3J(\omega_C) + 6J(\omega_H + \omega_C)] \quad (6)$$

where n is the number of attached protons and ω_C and ω_H are the Larmor (angular) frequencies of the ^{13}C and ^1H nuclei, respectively. The corresponding gyromagnetic ratios are given as γ_C and γ_H, respectively. The constant K is given by[32]

$$K = \frac{\hbar^2 \mu_0^2 \gamma_H^2 \gamma_C^2 \langle r_{CH}^{-3} \rangle^2}{160\pi^2} \qquad (7)$$

where μ_0 is the permittivity of free space and r_{CH} is the C−H bond length. K assumes values of 2.29×10^9 s^{-2} for sp^3 hybridized nuclei.[32] The spectral density function, $J(\omega)$, is given as[32]

$$J(\omega) = \frac{1}{2}\int_{-\infty}^{\infty} P_2^{CH}(t) \exp(i\omega t) \, dt \qquad (8)$$

Structure, Dynamics, and Thermodynamics of PEO

J. Phys. Chem. B, Vol. 107, No. 28, 2003 **6817**

TABLE 2: Density and Heat of Vaporization of PEO Oligomers from Experiments and MD Simulations Using Many-Body (MB) Polarizable Force Field FF-3, Including MB Polarization and Two-Body (TB) Nonpolarizable Force Field FF-3, Unless Indicated Otherwise

force field	temperature, T (K)	pressure, P (atm)	run length (ns)	Density, ρ (kg/m³)		Heat of Vaporization, ΔH (kcal/mol)	
				MD	experiment	MD	experiment
			Dimethyl Ether				
MB	254	1.35	0.9	679.3	715.6	4.93	5.05
TB	254	1.35	0.9	688.1	715.6	4.89	5.05
TB	293	5.24	0.9	631.2	661.0	4.50	4.61
			DME				
TB	298	1	5, 5,[a] 5[b]	850, 843,[a] 848[b]	861.3		
MB	298	1	8[a]	830[a]	861.3		
MB	318	1	1.2	824	840.8		
TB	318	1	8, 4,[a] 4[b]	826, 818[a] 822[c]	840.8		
TB	358	1	1.5	784		8.42	8.65
			Diglyme				
MB	293	1	1.5	938	943.4		
TB	293	1	1.5	942	943.4		
			PEO-500				
TB	300	1	15	1064	1069		
TB	318	1	42, 9,[b] 9[c]	1048, 1038[b] 1049[c]	1054		
TB	328	1	32, 16,[b] 18[c]	1039, 1030,[b] 1040[c]	1045		
TB	363	1	35, 6,[b] 6[c]	1012, 1002[b] 1013[c]			

[a] The average pressure over the entire NVT trajectories were found within 30 atm from the set pressure reported in the table. [a] For the FF-1 force field. [b] For the FF-2 force field.

where

$$P_2^{CH}(i,t) = \frac{1}{2}\{3\langle[e_{CH}(i,t) \cdot e_{CH}(i,0)]^2\rangle - 1\} \qquad (9)$$

Here, e_{CH} is a unit vector along a particular C–H bond, and the index i denotes differentiable resonances due to the local environment (methyl-, α-, and β-carbon atoms and interior carbon atoms).

F. Viscosity. The viscosity is calculated from MD simulations, using the Einstein relation[33]

$$\eta = \lim_{t\to\infty} \frac{V}{20k_BTt}\langle\sum_{\alpha\beta}(L_{\alpha\beta}(t) - L_{\alpha\beta}(0))^2\rangle \qquad (10)$$

where $L_{\alpha\beta}(t) = \int_0^t P_{\alpha\beta}(t')\,dt'$, k_B is the Boltzmann constant, T is the temperature, t is the time, $P_{\alpha\beta}$ is the symmetrized stress tensor, and V is the volume of the simulation box.

VI. Results and Discussion

A. Thermodynamic Properties. Densities of the ethylene oxide oligomers from the many-body (MB) polarizable force field and two-body (TB) nonpolarizable force field are compared with available experimental data[34–37] in Table 2. The dispersion parameters in the force field were adjusted to reproduce the density of diglyme for the force fields; thus, the simulation density of diglyme is in good agreement with the experimental density. The density of the PEO-500 is within 0.5%–1.5% of the experimental data, whereas predicted DME densities are within 1%–2.8% of the experimental values. The force fields (FF-2 and FF-3) predict the densities of dimethyl ether on the saturation curve with the worst accuracy (3.8%–5%).

Also shown in Table 2 is a comparison for the enthalpies of vaporization. The MD simulations predict enthalpies of vaporization within 3.3% of the experimental values. This agreement is considered excellent, because the experimental heats of vaporization were not used during the parametrization of the
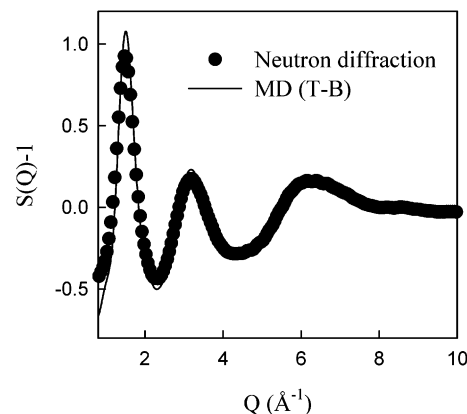

Figure 2. Static normalized coherent structure factor $S(Q)$ from neutron diffraction experiment and MD simulations.

force field. MD simulations with the MB polarizable force fields yield densities and heats of vaporization that are within 1% of the data from the simulations with the TB nonpolarizable force fields, which indicates that inclusion of the many-body polarizability is not important for prediction of the density and the heat of vaporization.

B. PEO Structure. Neutron diffraction experiments performed on high-molecular-weight PEO at 363 K are described in detail in ref 10. The structure factor from our previous MD simulations of the nonpolarizable force field with the different charges and valence potential was found in excellent agreement with the neutron diffraction data of Annis et al.[11] We calculated the structure factor for the current nonpolarizable and MB polarizable force fields using eq 2. The coherent static structure factor $S(Q)$ from MD simulations, using all force fields, and the neutron diffraction experiment are shown in Figure 2. The $S(Q)$ functions from MD simulations using FF-1, FF-2, and FF-3 MB polarizable force fields and TB nonpolarizable force fields are almost indistinguishable from each other; therefore, for clarity, only one data set is shown in Figure 2. The agreement between the experimental $S(Q)$ function and that from the MD

TABLE 3: Populations of DME Liquid and Gas Phases from MD Simulations and Liquid DME from IR Experiments at 298 K

	Population of Phases				
	FF-1 TB liquid, (FF-1 TB gas phase)	FF-1 MB liquid, (FF-1 MB gas phase)	FF-2 TB liquid	FF-3 TB liquid	liquid DME population, from IR experiment
conformer					
ttt	16.1 ± 1.4, (24.2 ± 2.8)	10.1 ± 1.3, (24.1 ± 2.9)	10.5 ± 1.2	15.0 ± 1.6	12
tgt	36.5 ± 1.9, (24.3 ± 2.2)	46.2 ± 2.1, (26.2 ± 1.9)	42.1 ± 2.3	49.0 ± 2.3	49
tg^+g^-	17.5 ± 1.0, (26.7 ± 2.7)	17.3 ± 1.1, (27.0 ± 2.8)	18.3 ± 1.2	14.5 ± 1.2	33
tgg	12.2 ± 1.0, (5.7 ± 1.0)	14.9 ± 1.3, (6.0 ± 1.2)	15.6 ± 1.3	11.2 ± 1.1	11
ttg	11.7 ± 1.1, (13.5 ± 1.9)	6.7 ± 1.0, (11.9 ± 1.5)	8.0 ± 1.0	7.4 ± 0.9	7
$\sigma(\text{MD-IR})^b$	7.0	2.6	4.2	1.5	

[a] Standard deviation for 100 ps block averages are given as the error. [b] Mean-square deviations of MD populations from IR populations (σ(MD-IR)) for the ttt, tgt, tgg, and ttg conformers are also given as percentages.

simulations is very good, further validating the developed PEO force field.

C. Conformations of PEO and Its Oligomers. We proceed with investigation of the influence of many-body polarizable interactions on DME in the gas and liquid phases. Conformational populations of DME in the gas phase from MD simulations using the FF-1 TB and MB force fields are shown in Table 3. They are essentially the same, within the errors shown, which indicates that the inclusion of the many-body polarization results in insignificant changes of the gas-phase populations and, therefore, relative conformational free energies. This is in agreement with the small (<0.2 kcal/mol) contribution of polarization to the relative conformational energetics that has been found in molecular mechanics studies.[1] Conformational populations of DME liquid from MD simulations with the TB force field, however, were found different from those with the MB force field, as seen in Table 3. The inclusion of polarization resulted in a more significant stabilization of the tgg and, especially, tgt conformers in DME liquid, compared to the gas phase, and destabilization of the ttt, tg^+g^-, and ttg conformers. Interestingly, a slight increase of the DME dipole moment and the magnitude of the electrostatic potential around DME in the FF-2 force field, compared to the FF-1 force field, also stabilizes tgt and tgg conformers in the liquid phase, in comparison that in to the gas phase, suggesting that the increased coulombic interaction can be used to capture the effect of the many-body polarization on conformational populations in the condensed phase in a mean-field sense.

Conformational populations for the most-important DME conformers from MD simulations of DME liquid at 298 K are compared to those estimated from the analysis of IR spectra at 300 K.[38] Excellent agreement between the conformers predicted from MD simulations and those from IR spectra is seen for the ttt, tgt, tgg, and ttg conformers. The FF-1 MB and FF-3 force fields yield the best agreement with mean-squared deviations of MD values from IR estimates of 2.6% and 1.5%. The FF-1 TB force field yields somewhat worse agreement, because turning off the polarization resulted in underestimation of the tgt stabilization in the condensed phase, compared to that in the gas phase. The only conformer where a significantly different population from IR experiments is predicted by the MD simulations is the tg^+g^- conformer. The difference between the MD results and analysis of the IR spectra for the tg^+g^- was attributed[38] to overestimation in the MD simulations of the intermolecular CH...O interaction, which is responsible for destabilization of the tg^+g^- in the liquid phase, relative to the bulk phase. We believe that overestimation of the intermolecular CH...O interaction is rather unlikely, because the force field binding energy of the dimethyl ether dimer is rather sensitive to the intermolecular CH...O interaction, which was found to be in excellent agreement with the high-level quantum chemistry

calculations, as shown in Figures 6 and 7 in the previous paper.[1] However, it is possible that this difference may be due to a large change in IR intensity for the tg^+g^- conformer upon transferring DME from the gas phase to the liquid phase.

The characteristic ratio of PEO serves as a measure of global polymer dimensions. At 393 K, the characteristic ratio of PEO ($M_w = 2380$) was found to be 5.9 ± 0.4 for the FF-3 TB force field. It is in good agreement with the experimental value of 5.3−5.9 at 363 K from recent SANS experiments[10] and the value of 5.6 from other SANS measurements[9] at 390 K, which indicates that the global PEO conformations are realistically represented by the present force field. The trajectories from MD simulations with the FF-1 and FF-2 MB force fields are less than half of the PEO Rouse time and, therefore, are unreliable for determination of the global PEO dimensions.

D. Dynamic Properties of PEO Oligomers. The self-diffusion coefficient of dimethyl ether has been measured as a function of temperature and pressure by pulse-field-gradient (PFG) spin−echo NMR.[39] The dimethyl ether self-diffusion coefficient, as a function of pressure and temperature, was calculated from MD simulations using the Einstein relationship, namely the slope of the plot of the center-of-mass mean-square displacement versus time divided by 6. The self-diffusion coefficients from the MD simulations with the MB and TB force fields are compared with the NMR data in Figure 3. MD simulations with both force fields yield self-diffusion coefficients that are in excellent agreement with the experimental data; the maximum deviation of the MB force field from the experimental data was 7.8%, whereas the two-body potential showed deviations of >12%. The difference between the MD simulations predictions using the MB and TB force fields is very small.

Incoherent quasi-elastic neutron scattering (QNS) experiments of hydrogenated polymers probe hydrogen motion. The most direct comparison between the experiment and simulations is achieved by comparing the ISF $I(Q,t)$ functions, which are obtained from the QNS experiment, with those calculated from the MD simulations. Because scattering from hydrogen is the dominant contribution, and it is essentially entirely incoherent scattering, only the incoherent ISF is relevant. The ISFs from MD simulations were calculated using eq 3, whereas the time Fourier transform of the experimentally measured dynamic structure factor $S(Q,\omega)$ yields the ISFs from QNS measurements. Unlike the QNS experiments, NSE experiments measure the ISF $I(Q,t)$ function directly.

A comparison of the incoherent ISF for DME at 318 K obtained from MD simulations and QNS experiments performed on the DCS is shown in Figure 4. Good agreement between the MD simulations for all force fields and QNS data is observed, with MD simulations predicting a decay of ISF that is up to 20% slower than the QNS experiments for the lowest value of Q investigated. Simulations with the MB force field
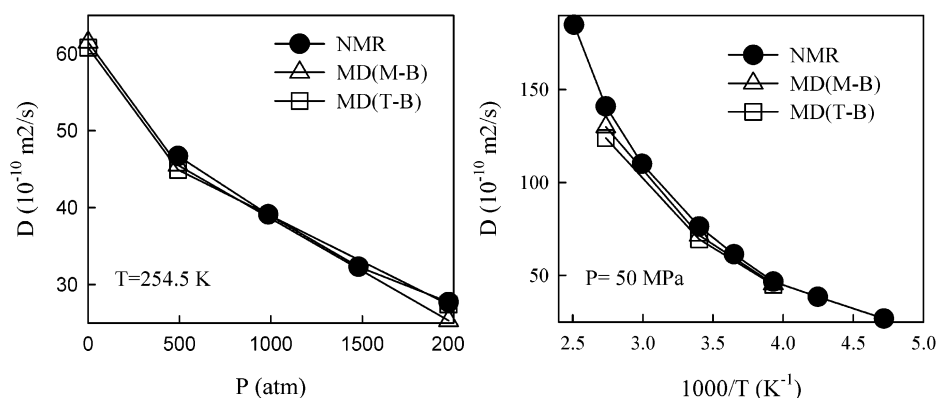
Figure 3. Self-diffusion coefficient (*D*) of dimethyl ether as a function of temperature (right) and pressure (left) from MD simulation and NMR experiments.[39]
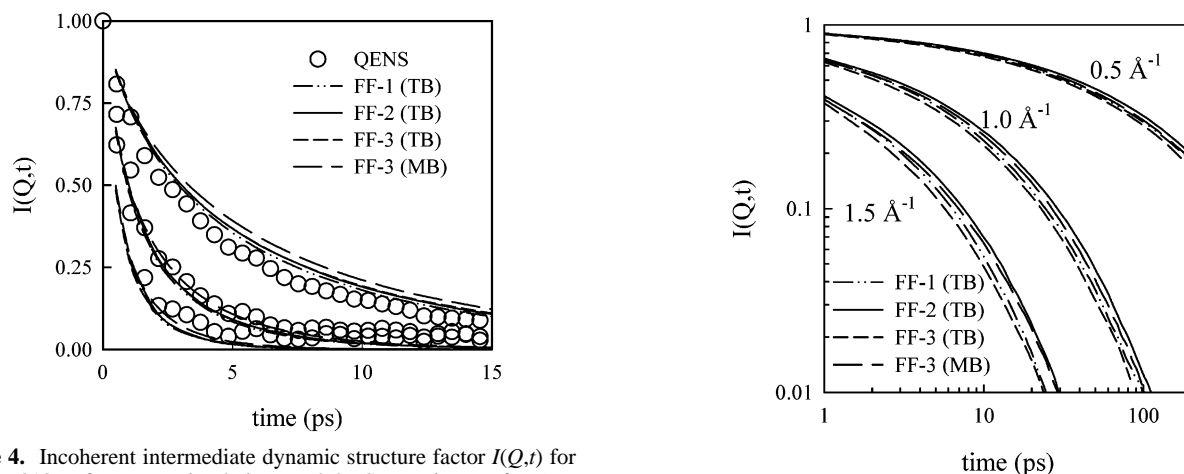

Figure 4. Incoherent intermediate dynamic structure factor $I(Q,t)$ for DME at 318 K from MD simulations and QNS experiments for $Q = 0.575, 0.909,$ and 1.227 Å^{-1}.

Figure 5. Incoherent intermediate dynamic structure factor $I(Q,t)$ for PEO ($M_w = 2380$) at 393 K for the two-body (TB) and many-body (MB) force fields.

yield a slightly slower (within 8%) decay of ISF, compared to the corresponding TB force field, which indicates that inclusion of the many-body polarizable interactions results in some, but insignificant, slowing of the motion of short ethylene oxide oligomers. The DME ISF was also similar to that from MD simulations using the TB force fields with the quantum chemistry barriers (FF-1 and FF-2) and reduced barriers (FF-3), which indicates that the conformational barrier heights have little influence on DME dynamics.

The effect of the many-body polarizability interactions, the description of the electrostatic potential, and the differing barriers on PEO dynamics is further explored by comparing ISFs for high-molecular-weight PEO ($M_w = 2380$) from MD simulations with all developed force fields at 393 K, as shown in Figure 5. A rather high temperature was chosen, to ensure proper system equilibration. The decay of ISF from simulations using the TB FF-1 and FF-3 (FF-3 has reduced barriers but increased electrostatic potential around DME, compared to the same values for FF-1) force fields is the fastest, whereas the decay of the ISF from simulations using the TB FF-2 force field with original barriers but increased electrostatic potential around ether molecules is the slowest. Comparison of the time integrals of the ISF, i.e., relaxation times, for $Q = 1.0$ Å^{-1} revealed the following relation between the relaxation times: τ(FF-1 TB): τ(FF-2 TB):τ(FF-3 TB):τ(FF-3 MB) = 9.2:10.8:8.6:9.99 (in picoseconds) = 1.07:1.26:1.0:1.16. These relaxation times indicate that the inclusion of polarizability (MB vs TB) and the increase of the DME electrostatic potential (coulombic interactions) (FF-2 vs FF-1) both slow the polymer dynamics by ~16%, suggesting that the effect of the inclusion of

polarizability on PEO dynamics can be reasonably modeled by increasing the DME coulombic interactions, as was found for DME conformational populations. PEO dynamics with the MB and TB force fields are rather similar; therefore, we will use only the TB force fields from this point forward for investigation of the PEO dynamics at lower temperatures, because the computation of MD simulations of PEO with the TB force fields is ~3 times faster than that of those with the MB force fields.

The ISF for PEO-500 at 318 K obtained from MD simulations are shown in Figure 6a. The decay of the ISF is very similar for the FF-1 and FF-3 force fields, whereas the dynamics of FF-2 are ~35% slower, as a result of increased coulombic interactions, compared to those of FF-1. The FF-3 force field has the same coulombic interaction as the FF-2 force field but shows faster decay than the FF-2 force field, because of the reduction of torsional barriers. Results of QNS experiments using DCS are compared with MD simulations in Figure 6b. Neutron scattering simulations[15] have been applied to the MD data, to correct for any multiple scattering effects in the experiments. An excellent agreement between the ISFs from simulations and experiments unequivocally demonstrates the ability of the developed force fields (FF-1 and FF-3) to correctly reproduce PEO dynamics on a length scale of 3−12 Å and a time scale of 1−30 ps.

QNS experiments[40] on high-molecular-weight PEO ($M_w = 40\ 000$) and NSE experiments[14] on PEO ($M_w = 8000$) have also been previously performed, probing hydrogen dynamics on a time scale of 0.01−1.7 ns. The ISFs from these measure-
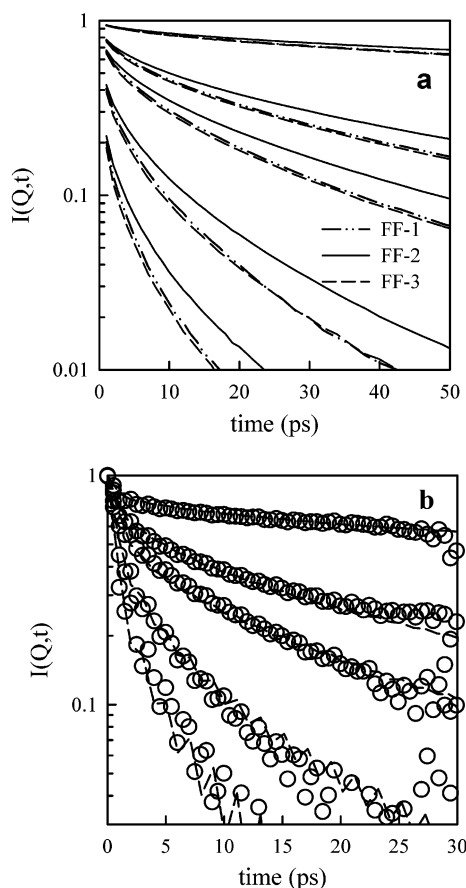
Figure 6. Incoherent intermediate dynamic structure factor $I(Q,t)$ for PEO-500 from MD simulations (a) using FF-1 force field (line) after multiple scattering correction and (b) from disk chopper spectrometer QNS experiments (symbols) for Q = 0.475, 0.913, 1.139, 1.716, and 2.174 Å^{-1}.

ments are compared with the results of MD simulations in Figure 7a, b. Both sets of experimental data predict a slower decay than do the MD simulations at short times and high Q-values, whereas faster decay at long times and low Q-values is observed in NSE and QNS experiments, compared to MD simulation predictions. MD simulations using the FF-1 and FF-3 force fields yield ISFs that show the best agreement with QNS experiments at long times. The NSE data shown in Figure 7b agree with the ISFs from the MD simulations slightly better than do the QNS data shown in Figure 7a. The dynamic correlation times were calculated as time integrals of the stretched exponential fits to ISFs from NSE experiments and MD simulations. Dynamic correlation times were ~20%−30% higher for ISFs from simulations using the FF-1 and FF-3 force field and 65% for the FF-2 force field, in comparison to the NSE experiments at $Q = 1$ Å^{-1}, indicating good agreement between the NSE experiment and MD simulations with the FF-1 and FF-3 force fields, and fair agreement for the FF-2 force field.

Dielectric spectroscopy of polymer molecules also allows one to probe polymer dynamics through Fourier transform of the dipole moment autocorrelation function (see eqs 4 and 5). The dielectric loss from MD simulations of PEO-500 is compared with the results of the dielectric spectroscopy measurements on PEO-500 with a similar molecular weight distribution in Figure 8a. Our MD simulations with the FF-2 force fields yield the best agreement with experiments, whereas the FF-1 and FF-3 force fields predict the position of the maximum dielectric loss to be shifted by 0.1 and 0.25 on a $\log_{10}$ scale toward higher frequencies, relative to the FF-2 force field results. Figure 8b
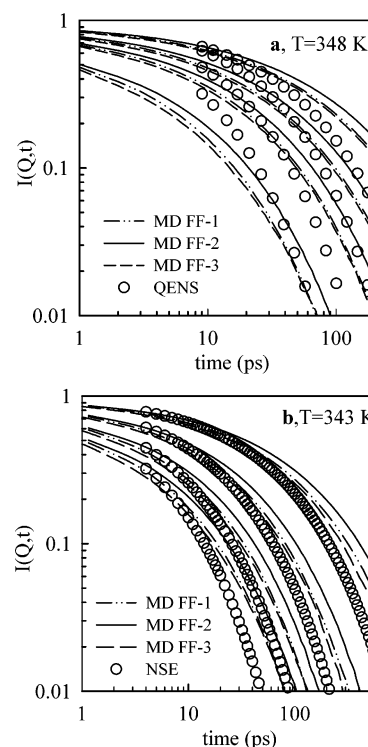

Figure 7. Incoherent intermediate dynamic structure factor $I(Q,t)$ for PEO ($M_w = 2380$) from MD simulations, compared with the results for high-molecular-weight PEO from (a) the QNS experiments for Q = 0.72, 0.91, 1.10, and 1.55 Å^{-1} at 348 K and (b) NSE experiments for Q = 0.7, 1.0, 1.3, and 1.55 Å^{-1} at 343 K.
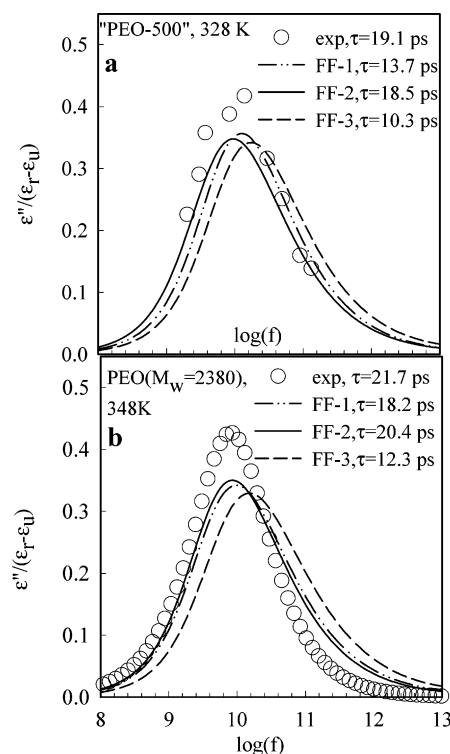

Figure 8. Normalized dielectric loss from the MD simulations for (a) PEO-500 and (b) PEO ($M_w = 2380$). Data from the dielectric spectroscopy experiments for PEO-500 and high-molecular-weight PEO have been taken from ref 41.

compares the dielectric loss of PEO ($M_w = 2380$) from MD simulations with that from the Cole−Cole fit to the dielectric spectroscopy measurements[41] that were performed for frequen-
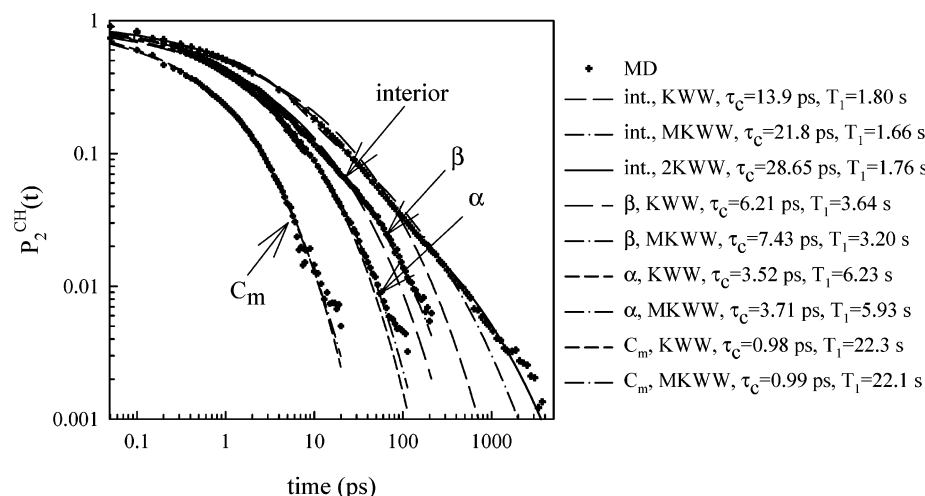
Structure, Dynamics, and Thermodynamics of PEO

J. Phys. Chem. B, Vol. 107, No. 28, 2003 **6821**

Figure 9. $P_2^{CH}(t)$ autocorrelation function for PEO (M_w = 2380) at 393 K from MD simulations using the force field with reduced barriers. KWW, MKWW, and 2KWW fits to data are shown, together with the CH-vector autocorrelation times (τ_c) and corresponding spin−lattice relaxation times (T_1).

cies lower than the frequency of the maximum of the loss of high-molecular-weight PEO (Carbowax 20M). As seen for PEO-500, the dielectric loss predictions from MD simulations using the FF-1 and FF-2 force fields show the best agreement with experiments, whereas the FF-3 force field predicts the maximum frequency position to be shifted by 0.26 toward higher frequencies, which indicates that the dielectric spectroscopy experiments are consistent with each other.[41] All the force fields predict a slightly broader relaxation spectrum than those for dielectric experiments, which is consistent with the more-stretched ISF functions that are predicted by MD, in comparison with NSE experiments.

Spin−lattice relaxation times T_1 that have been measured by ^{13}C NMR experiments also serve as a measure of polymer conformational motion through the decay of the C−H vector autocorrelation function (ACF) and the spectral density functions, as described by eqs 6−9. To evaluate the time integral (eq 8) and calculate the spectral density function $J(\omega)$ from MD simulations, we need to know the long-time behavior of the C−H vector ACF $P_2^{CH}(i,t)$. Figure 9 shows typical C−H vector ACFs, and we have attempted to fit the decay of the $P_2^{CH}(i,t)$ functions with the following functions: a stretched exponential, or KWW, expression, $\exp[-(t/\tau_{KWW})^\beta]$; a modified KWW (MKWW), given by $A \exp[-(t/\tau_{KWW})^\beta] + (1 - A) \exp[-(t/\tau_2)]$; and a sum of two KWW expressions, which is referenced as 2KWW. For the PEO (M_w = 2380) and PEO-500, we find that the decay of $P_2^{CH}(C_m,t)$ and $P_2^{CH}(\alpha,t)$ can be adequately represented by the KWW expression and the $P_2^{CH}(\beta,t)$ could be represented by the MKWW, whereas the 2KWW function is necessary to adequately represent decay of the $P_2^{CH}(interior\ carbon,t)$ function. Figure 9 illustrates that the C−H vector autocorrelation time, which is calculated as the time integral of the ACF, is sensitive to the functional form used for the approximation of $P_2^{CH}(t)$, whereas the T_1 spin−lattice relaxation time calculated using eqs 6−9 is less sensitive to the functional form that is used to approximate $P_2^{CH}(t)$. We estimated the uncertainty in the determination of the C−H vector autocorrelation time from MD simulations to be ∼20%−30%, whereas the uncertainty in T_1 is estimated at 10%−15%. For the MD simulations, the T_1 values (eqs 6−9) were calculated from the Fourier transforms of the KWW, MKWW, and 2KWW fits to the data.

The T_1 spin−lattice relaxation times for PEO-500 and PEO (M_w = 2380) from the MD simulations are compared with the
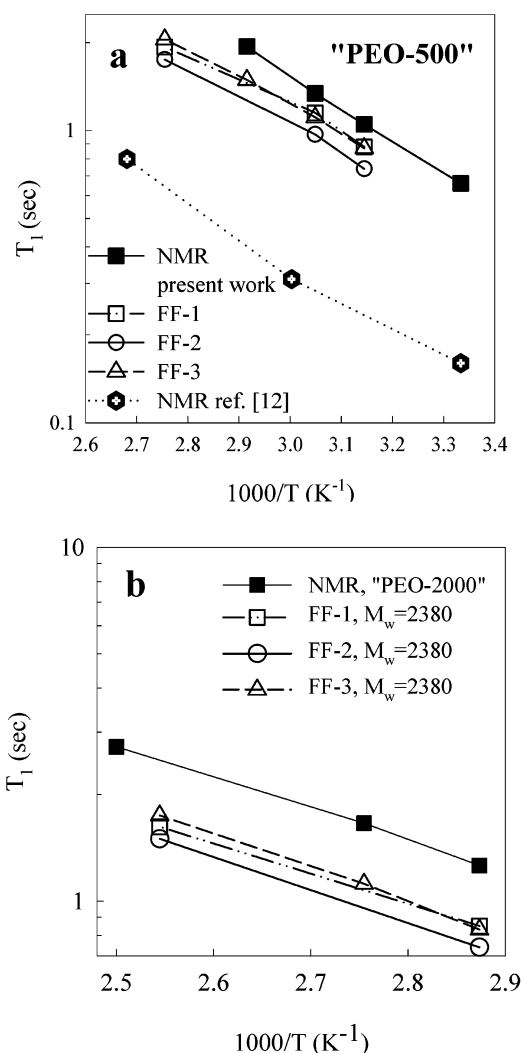

Figure 10. T_1 spin−lattice relaxation times for interior carbon atoms ((a) PEO-500 and (b) high-molecular-weight PEOs) from MD simulations using TB force fields and NMR experiments (closed symbols). Dotted line shows the T_1 spin−lattice relaxation times from the previous ^{13}C NMR experiments.[12]

500 MHz NMR results for PEO-500 and PEO (M_w = 1854) in Figures 10 and 11. Figure 10 indicates that the FF-1 and FF-3 force fields predict T_1 spin−lattice relaxation times in best
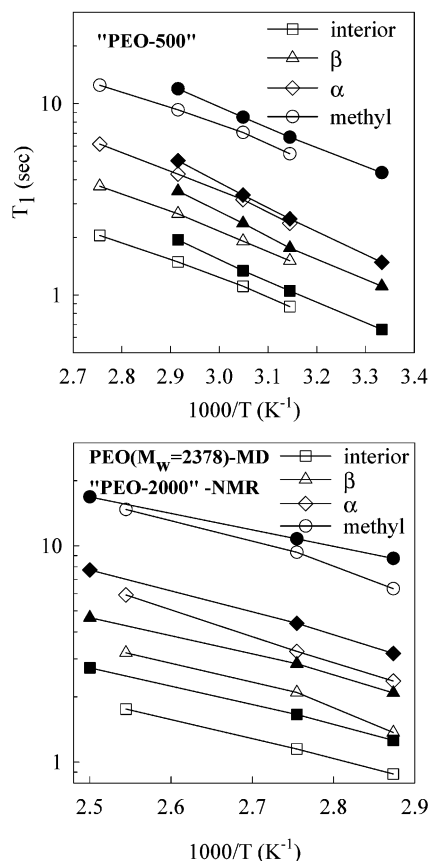
Figure 11. T_1 spin–lattice relaxation times from MD simulations using TB FF-3 (open symbols) and NMR experiments (closed symbols). Top figure represents data for PEO-500, and bottom figure represents data from high-molecular-weight PEOs.

agreement with experiments, while slightly underestimating experimental values by 15%−25% for PEO-500 and by ~30% for PEO (M_w = 2380). The FF-2 force field predicts slightly lower T_1 relaxation times (by 6%−10%) and higher C−H vector relaxation times (by 15%−20%) than the FF-1 and FF-3 force fields, which is consistent with the ISF for the corresponding force fields, as shown in Figures 5−7, but slightly different from the predicted tendencies of the dielectric behavior (Figure 8). Figure 10a also shows the results from the previous 300 MHz NMR study of PEO (M_w = 531)[12] that yielded T_1 spin−lattice relaxation times that are ~2 times lower than the present 500 MHz NMR data for PEO-500. Our estimates suggest that the difference in molecular weight between PEO-500 and PEO (M_w = 531) could account for up to 10% of the discrepancy in T_1, whereas the difference in frequency (300 MHz versus 500 MHz) accounts for a few percent at 363 K and <25% at 328 K, which indicates that the previous 300 MHz NMR T_1 data are inconsistent with the present NMR data. The present NMR data are in good agreement with the MD simulations predictions, which are also in good agreement with the QNS, NSE, and dielectric spectroscopy data; therefore, we conclude that the previous NMR data are inconsistent with all the experimental data on PEO dynamics that have been presented in this paper.

The motion of the carbon atoms located at PEO ends (methyl, α, and β carbon atoms) predicted by the MD simulations also agrees well with that probed through T_1 spin-lattice relaxation times in NMR experiments, as seen in Figure 11, which indicates that the FF-3 TB force field can capture the dynamics of the end groups. Similar T_1 spin−lattice relaxation times have been observed for the other force fields.
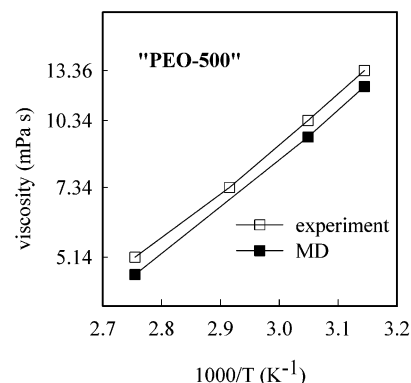

Figure 12. Viscosities of PEO-500 from the MD simulations using the FF-3 TB force field and from experiments.

E. PEO Viscosity. The viscosity (η) of DME and PEO-500 has been measured experimentally, and is accessible from MD simulations. The viscosity was calculated in MD simulations for DME using TB FF-1, FF-2, and FF-3 force fields, yielding DME viscosities of 0.41, 0.43, and 0.40 mPa·s at 298 K, respectively, which is in good agreement with the experimental value of 0.424 mPa·s. This is consistent with the accurate prediction of DME dynamics by MD simulations, as demonstrated by the agreement between MD and the QNS experiments shown in Figure 4. The independence of the DME viscosity from the barrier heights (FF-3 vs FF-2) indicates that, unlike that for PEO-500 and PEO (M_w = 2380), torsional barriers play a minor role in DME transport and diffusion.

The viscosity of PEO-500, as a function of temperature, was also calculated from the MD simulations, using the TB FF-3 with reduced barriers, and this is shown in Figure 12, together with the experimental data. The viscosities predicted by MD simulations are only ~8%−10% below the PEO-500 viscosities that have been derived from experiments, further validating the force field used. Viscosities have not been calculated for the other force fields, because this type of calculation requires the generation of long trajectories and is computationally expensive.

VII. Conclusions

Molecular dynamics (MD) simulations have been performed on poly(ethylene oxide) (PEO) and its oligomers, using many-body (MB) polarizable and two-body (TB) nonpolarizable force fields with different sets of partial charges representing coulombic interactions. The effects of polarizability on polymer structure, conformations, and thermodynamic properties have been investigated. We found that the inclusion of polarization interaction in the dimethoxyethane (DME) model resulted in a larger stabilization of the tgg and, especially, tgt conformers in the liquid, compared to the gas phase, and destabilization of the ttt, tg$^+$g$^-$, and ttg conformers. Increasing the DME coulombic interactions also led to larger stabilization of the tgg and tgt conformers. The inclusion of polarization and the increase of dipole moments slowed the polymer dynamics from 5% to 30%, depending on the molecular weight of the polymer and the temperature. Therefore, we conclude that inclusion of polarizability has a minor effect on the prediction of PEO melt conformational, structural, and dynamic properties. However, we will show in the next paper[2] that the inclusion of polarizability in the PEO model is important for modeling polymer electrolytes, such as PEO/LiBF$_4$.

We also show that the quantum chemistry-based FF-1 force field, which contains no adjustable empirical parameters, yields structural, dynamic, thermodynamic, and transport properties

Structure, Dynamics, and Thermodynamics of PEO

J. Phys. Chem. B, Vol. 107, No. 28, 2003 **6823**

that are in good agreement with the experiment, validating the present methodology of force field development. Unfortunately, this force field underestimates the PEO electrostatic potential in the proximity of PEO, making its use for simulations of polymer electrolytes questionable. The FF-2 force field, on the other hand, provided a good description of the PEO electrostatic potential in the proximity of PEO, which promises better applicability to PEO/Li salt simulations; however, it predicts slower dynamics, in comparison to the FF-1 force field results and experiments, which indicates that slower-than-expected ion and polymer dynamics in polymer electrolytes will be predicted by this force field. Empirical reduction of torsional barriers to accelerate polymer motion, while keeping a set of charges that are required for the accurate description of the PEO−cation complexation, is one of the avenues for getting improved PEO force field for simulations of polymer electrolytes. The FF-3 force field incorporates this empirical adjustment and is recommended for future MD simulations of the PEO-based polymer electrolytes.

Finally, in this contribution, we have demonstrated that the previous ^{13}C NMR experiment yielded T_1 spin−lattice relaxation times that were a factor of ∼2 lower than those reported in this work. The new T_1 relaxation times were found to be consistent with the quasi-elastic neutron scattering, neutron spin−echo spectroscopy, and dielectric spectroscopy data by direct comparison with MD simulations results, and by the implication that the previous NMR results are inconsistent with all these experiments.

References and Notes

(1) Borodin, O.; Smith, G. D. *J. Phys. Chem. B*, **2003**, *107*, 6824.
(2) Borodin, O.; Smith, G. D.; Douglas, R. *J. Phys. Chem. B*, **2003**, *107*, 6824.
(3) Halley, J. W.; Duan, Y.; Nielsen, B.; Redfern, P. C.; Curtiss, L. A. *J. Chem. Phys.* **2001**, *115*, 3957.
(4) Lin, B.; Halley, J. W.; Boinske, P. T. *J. Chem. Phys.* **1996**, *105*, 1668.
(5) Smith, G. D.; Jaffe, R. L.; Yoon, D. Y. *J. Phys. Chem.* **1993**, *97*, 12752.
(6) Neyertz, S.; Brown, D.; Thomas, J. O. *J. Chem. Phys.* **1994**, *101*, 10064.
(7) Müller-Plathe, F.; van Gunsteren, W. F. *J. Chem. Phys.* **1995**, *103*, 4745.
(8) Hyun, J.-K.; Dong, H.; Rhodes, C. P.; Frech, R.; Wheeler, R. A. *J. Phys. Chem. B* **2001**, *10*, 3329.
(9) Smith, G. D.; Yoon, D. Y.; Jaffe, R. L.; Colby, R. H.; Krishnamoorti, R.; Fetters, L. J. *Macromolecules* **1996**, *29*, 3462.
(10) Annis, B. K.; Kim, M.-H.; Wignall, G. D.; Borodin, O.; Smith, G. D. *Macromolecules* **2000**, *33*, 7544.
(11) Annis, B. K.; Borodin, O.; Smith, G. D.; Benmore, C. J.; Soper, A. K.; Londono, J. D. *J. Phys. Chem.* **2001**, *115*, 10998.
(12) Smith, G. D.; Yoon, D. Y.; Wade, C. G.; O'Leary, D.; Chen, A.; Jaffe, R. L. *J. Chem. Phys.* **1997**, *106*, 3798.
(13) Neyertz, S.; Brown, D.; Thomas, J. O. *Comput. Polym. Sci.* **1995**, *5*, 107.
(14) Mos, B.; Verkerk, P.; Pouget, S.; van Zon, A.; Bel, G.-J.; de Leeuw, S. W.; Eisenbach, C. D. *J. Chem. Phys.* **2000**, *113*, 4.
(15) Trouw, F.; Borodin, O.; Cook, J. C.; Copley, J. R. D.; Smith, G. D. *J. Phys. Chem. B*, in press.
(16) Bradley, K. F.; Chen, S.-H.; Brun, T. O.; Kleb, R.; Loomis, W. A.; Newsam, J. M. *Nucl. Instrum. Methods Phys. Res., Sect. A* **1988**, *A270*, 78.
(17) Trouw, F.; Bedrov, D.; Borodin, O.; Smith, G. D. *Chem. Phys.* **2000**, *261*, 137.
(18) Farber, H.; Petrucci, S. *J. Phys. Chem.* **1975**, *79*, 1221.
(19) Delsignore, M.; Farber, H.; Petrucci, S. *J. Phys. Chem.* **1985**, *89*, 4968.
(20) Lucretius; www.che.utah.edu/∼gdsmith.
(21) Smith, G. D.; Jaffe, R. L; Yoon, D. Y. *Macromolecules* **1993**, *26*, 298.
(22) Allen, M. P.; Tildesley, D. J. *Computer Simulation of Liquids*; Oxford University Press: New York, 1987.
(23) Nose, S. In *Computer Simulation in Materials Science*; Meyer, M., Pontikis, V., Eds.; Kluwer Academic Publishers, Amsterdam, 1991; p 21.
(24) Martyna, G. J.; Tuckerman, M.; Tobias, D. J.; Klein, M. L. *Mol. Phys.* **1996**, *87*, 1117.
(25) Ryckaert, J. P.; Ciccotti, G.; Berendsen, H. J. C. *J. Comput. Phys.* **1977**, *23*, 327.
(26) Kittel, C. *Introduction to the Theory of Solids*, 2nd ed.; Wiley: New York, 1956; Appendix A.
(27) Deserno, M.; Holm, C. *J. Chem. Phys.* **1998**, *109*, 7678.
(28) Steinhauser, O. *Mol. Phys.* **1982**, *45*, 335.
(29) Martyna, G. J.; Tuckerman, M.; Tobias, D. J.; Klein, M. L. *Mol. Phys.* **1996**, *87*, 1117.
(30) Higgins, J. S.; Benoît, H. C. *Polymers and Neutron Scattering*; Clarendon Press: Oxford, U.K., 1996.
(31) Edwards, D. M. F.; Madden, P. A.; McDonald, I. R. *Mol. Phys.* **1984**, *51*, 1141.
(32) Gisser, D. J.; Glowinkowski, S.; Ediger, M. D. *Macromolecules* **1991**, *24*, 4270.
(33) Haile, J. M. *Molecular Dynamics Simulations*; Wiley: New York, 1992.
(34) Das, B.; Roy, M. N.; Hazra, D. K. *Indian J. Chem. Technol.* **1994**, *1*, 93.
(35) Lide, D. L. *Handbook of Organic Solvents*; CRC Press: London, Tokyo, 1995.
(36) Flick, E. W. *Industrial Solvent Handbook*, 5th ed.; Noyes Data Corporation, Westwood, NJ.
(37) Densities of "PEO-500" at 298 and 328 K have been measured, whereas those at the other temperatures were obtained by linear interpolation of the experimental data at 298 and 328 K.
(38) Goutev, N.; Ohno, K.; Matsuura, H. *J. Phys. Chem. A* **2000**, *104*, 9226.
(39) Heinrich-Schramm, A.; Price, W. E.; Lüdemann, H.-D. *Z. Naturforsch.*, **1995**, *50a*, 145.
(40) Saboungi, M.-L.; Price, D. L.; Mao, G.; Fernandez-Perea, R.; Borodin, O.; Smith, G. D.; Armand, M.; Howells, W. S. *Solid State Ionics* **2002**, *147*, 225.
(41) Porter, C. H.; Boyd, R. H. *Macromolecules* **1971**, *4*, 589.